Simulation of Deployable Cable Nets for Active Debris Removal in Space

Simulation of Deployable Cable Nets for Active Debris Removal in Space

Paolo Fisicaro, Angelo Pasini, Paolo S. Valvo

University of Pisa, Department of Civil and Industrial Engineering, Largo Lucio Lazzarino, I-56122 Pisa, PI, Italy

E-mail: paolo.fisicaro@ing.unipi.it

Abstract. Deployable cable nets have been proposed as promising systems for the active removal of space debris. The modelling and analysis of such systems during deployment, capture, and post-capture phases are crucial for the effective design of an operative mission. To this aim, accurate and effective simulation tools are necessary. We propose a finite element model of the cable net with lumped nodal masses and first-order cable elements. The nodal positions are assumed as the main unknowns of the problem. The large displacements and finite deformations are described by the Green-Lagrange strain tensor. The cable elements are assumed to react only in tension. Global damping is considered in line with Rayleigh's hypothesis. The governing equations are solved numerically by means of the Runge-Kutta method with a variable time step. As an illustrative example, we present the simulation of the in-plane deployment of a planar, square-mesh net. The proposed approach turns out to be computationally effective, even if the accuracy of the numerical integration scheme needs to be improved, particularly in the final stages of deployment.

1. Introduction

Missions in the circumterrestrial space produce debris that represents a threat to current and future space activities. Even the impact of small- and medium-sized debris may cause malfunctions and reduce the functional lifetime of operational satellites. The impact of large debris would determine a complete destruction of impacting bodies with a production of new fragments [1]. In the worst-case scenario, a series of catastrophic collisions would originate a cascade effect, ending up with the creation of a belt of debris around the Earth [2, 3].

Once the main national space agencies became aware of the problem, they have developed and adopted mitigation guidelines to reduce the debris production rate from new missions [4, 5]. However, the overall number of space debris is steadily increasing because of increasing space activities [6, 7], and the same is happening to costs related to space debris – from damages, constraints in satellite design, surveillance activities, and insurance fees [8]. As a consequence, remediation activities must be set up to guarantee access to space for future generations. In particular, the disposal of massive objects abandoned around the Earth would result effective to secure the most valuable orbital regions [6, 9, 10].

Many methods and strategies for the removal of space debris have been proposed, most of which remain theoretical [11, 12]. For active debris removal (ADR), the development of an effective capturing mechanism is still one of the most problematic aspects of the mission architecture. Two main alternatives have been considered: robotic arms and tethered nets.

In the last twenty years, both the Space Shuttle and the International Space Station have been equipped with robotic arms. Indeed, robotic arms have been effectively used to capture cooperative and attitude-stabilised spacecrafts, both under human control and by automated procedures [13]. Anyhow, their efficacy for the capture of non-cooperative debris still has to be proven. In fact, the complexity of approaching manoeuvres can be guessed if we consider a tumbling target with large appendages, from which a distance between 1 and 3 meters has to be reached. For comparison, cable nets can be thrown from distances of 20 meters. Also, they are light, easily packable, scalable, and versatile. Nonetheless, guidance, navigation, and control (GNC) aspects are especially critical for nets in the capture and post-capture phases [11, 12].

In a typical ADR mission, the chaser will first operate a rendez-vous with the target and then throw a tethered net to capture debris. The deployment of the net can be achieved by ejecting a number of bullet masses placed on the border of the net. When cables connected to the bullets start tensioning, they pull along neighbouring portions of the net, while the initial kinetic energy stored in the bullet masses is partly converted into elastic potential energy stored in cables.

The development of accurate and effective simulation tools is crucial to enable the real application of cable nets in ADR missions. Several theoretical models have been proposed to describe deployment and capture processes. Benvenuto et al. [14] and Botta et al. [15] modelled the net as a system of concentrated masses – including both the bullet masses and nodal masses representative of the cables – connected to each other by spring-dampers. In their models, springs react only in tension with a linear stress-strain relationship between the infinitesimal strain and Cauchy stress tensors. Shan et al. [16] compared the simple lumped mass-spring model with a more refined model based on the absolute nodal coordinate formulation (ANCF) proposed by Shabana [17]. Here, cables are modelled through a third-order cable element [18], whereas finite strains are described by the Green-Lagrange strain tensor. Compressive stresses are allowed in cables which, however, may buckle because of their little bending stiffness. The lumped mass-spring and ANCF models gave similar results in terms of the overall behaviour of the net, but the ANCF model was much more computationally expensive.

We propose a finite element (FE) model of a cable net with lumped nodal masses and first-order cable elements. In line with the ANCF, we assume nodal positions as the main unknowns of the problem instead of nodal displacements which are commonly adopted in finite element analysis [19]. As a result, the elastic secant stiffness matrix of the system turns out to be symmetric [20]. The large displacements and finite deformations are described by the Green-Lagrange strain tensor. The cable elements are assumed to react only in tension with a linear relationship between the axial strain and the corresponding component of the work-conjugate second Piola-Kirchhoff stress tensor [21]. Global damping is introduced into the model according to Rayleigh's hypothesis [22]. The governing equations are solved numerically by means of the Runge-Kutta method with a variable time step within the MATLAB software environment [23].

As a very first illustrative example, we present the simulation of the in-plane deployment of a planar, square-mesh net already investigated by Botta et al. [15]. The numerical example intentionally disregards some issues – such as gravitational and centrifugal forces – which will be included in future simulations. Besides, the theoretical model shall be improved to account for the contact phenomena arising after the impact of the net with the target.

The proposed approach turns out to be computationally effective, even if the accuracy of the numerical integration scheme needs to be improved, particularly in the final stages of deployment. In the future, our model can be used to compare several net configurations as well as to design throwing conditions appropriate for the desired performances.

2. Finite element formulation

2.1. Kinematics

The deployable cable net is modelled in the framework of the finite element method [19]. Accordingly, a continuous mechanical system is modelled as a discrete system consisting of m elements of finite size, connected to each other at n points called nodes. All the mass, damping, and elastic properties as well as the applied loads and restraints, which may be distributed in the original mechanical system, are modelled as lumped nodal entities in the discretised FE model. In the case of the cable net, the nodes are naturally located at the intersections between the cables, and the elements correspond to the portions of the cables included between them.

The geometry of the system is described in the Euclidean space, $\mathcal{E}$, of dimension $d = 3$ (Fig. 1). Here, a Cartesian reference system, $Ox_1x_2x_3$, is fixed so that physical vectors can be represented in terms of their scalar components as column vectors of $\mathbb{R}^3$. Let $P_1, P_2, \ldots, P_n \in \mathcal{E}$ denote the points corresponding to the node positions in a given (current) configuration. Accordingly, $\mathbf{x}_i = P_i - O \in \mathbb{R}^3$ denotes the position vector of the i^{th} node ($i = 1, 2, \ldots, n$).

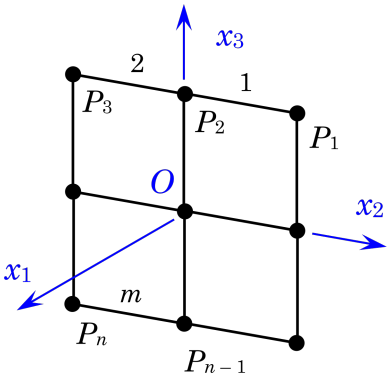

Figure 1. FE model of the cable net.

Among the many possible configurations of the system, we choose a particular one as the reference configuration. Here, let $\bar{P}_1, \bar{P}_2, \ldots, \bar{P}_n$ be the points corresponding to the node positions and $\bar{\mathbf{x}}_i = \bar{P}_i - O \in \mathbb{R}^3$ the nodal position vector of the i^{th} node. The displacement vector of the i^{th} node is defined as $\mathbf{u}_i = P_i - \bar{P}_i = \mathbf{x}_i - \bar{\mathbf{x}}_i \in \mathbb{R}^3$. It is worth noting that the reference configuration need not be the one occupied by the system initially or at any subsequent instant of time. However, the reference configuration is by definition undeformed. Thus, if we exclude the presence of any self-stress, it will be also unstressed.

The position vectors of all of the n nodes of the system in the reference and current configurations are collected into vectors $\bar{\mathbf{x}} = [\bar{\mathbf{x}}_1; \bar{\mathbf{x}}_2; \ldots; \bar{\mathbf{x}}_n] \in \mathbb{R}^{3n}$ and $\mathbf{x} = [\mathbf{x}_1; \mathbf{x}_2; \ldots; \mathbf{x}_n] \in \mathbb{R}^{3n}$, respectively. In the standard finite element formulation, the displacement vector, $\mathbf{u} = [\mathbf{u}_1; \mathbf{u}_2; \ldots; \mathbf{u}_n] = \mathbf{x} - \bar{\mathbf{x}} \in \mathbb{R}^{3n}$, is assumed as the main unknown [19]. In the present work, we alternatively use the nodal position vector in the current configuration, $\mathbf{x}$ [17, 20].

2.2. Cable element formulation

The cable elements are formulated from the first-order truss bar element described by Valvo [20] by the introduction of a suitable constitutive law. Let us consider the cable element, labelled e ($e = 1, 2, \ldots, m$), connecting two nodes numbered as i and j. Let $\bar{\Omega}_e$ and Ω_e denote the regions of $\mathcal{E}$ occupied by the element in the reference and current configurations, respectively. Besides, let $\bar{A}_e$, $\bar{L}_e$ and A_e, L_e denote the element cross-section area and length in $\bar{\Omega}_e$ and Ω_e, respectively (Fig. 2).

Within each element, the displacement of a point, $\bar{P} \in \bar{\Omega}_e$, with a position vector $\bar{\mathbf{x}}_P =$

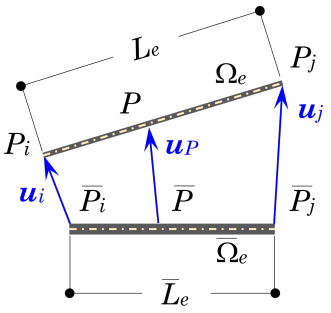

Figure 2. Cable element in the reference and current configurations.

$\bar{P} - O \in \mathbb{R}^3$, is approximated as

$$\mathbf{u}_P \cong \mathbf{N}_e\left(\bar{\mathbf{x}}_P\right)\mathbf{u}_e, \tag{1}$$

where $\mathbf{N}_e\left(\bar{\mathbf{x}}_P\right) \in \mathbb{R}^{3\times 6}$ and $\mathbf{u}_e = [\mathbf{u}_i;\mathbf{u}_j] \in \mathbb{R}^6$ respectively are the shape function matrix and nodal displacement vector of the element. In turn, the element nodal displacement vector can be expressed as

$$\mathbf{u}_e = \mathbf{A}_e\mathbf{u}, \tag{2}$$

where $\mathbf{A}_e \in \mathbb{R}^{6\times 3n}$ is the assembly matrix of the element. This matrix is defined as a null matrix, except for rows 1 to 3, columns $3i-2$ to $3i$ and rows 4 to 6, columns $3j-2$ to $3j$ where the identity matrices $\mathbf{I} \in \mathbb{R}^{3\times 3}$ are placed. The assembly matrix is here introduced to explain the analytical formulation. However, for numerical implementation, it is more computationally effective to code the assembly process via the direct extraction of the sub-vectors and sub-matrices corresponding to the involved nodes.

For what follows, it is also useful to introduce the nodal position vectors of the element, $\bar{\mathbf{x}}_e = [\bar{\mathbf{x}}_i;\bar{\mathbf{x}}_j] = \mathbf{A}_e\bar{\mathbf{x}} \in \mathbb{R}^6$ and $\mathbf{x}_e = [\mathbf{x}_i;\mathbf{x}_j] = \mathbf{A}_e\mathbf{x} \in \mathbb{R}^6$, in the reference and current configurations, respectively.

By assuming linear shape functions for the element, the secant elastic stiffness matrix can be expressed as follows [20]:

$$\mathbf{S}_e\left(\mathbf{x}_e\right) = S_{11}\frac{\bar{A}_e}{\bar{L}_e}\mathbf{\Delta}, \tag{3}$$

where S_{11} is the component of the second Piola-Kirchhoff stress tensor in the element axial direction [21] and

$$\mathbf{\Delta} = \begin{bmatrix} \mathbf{I} & -\mathbf{I} \\ -\mathbf{I} & \mathbf{I} \end{bmatrix} \tag{4}$$

is a constant matrix. Besides, the tangent elastic stiffness matrix is

$$\mathbf{T}_e\left(\mathbf{x}_e\right) = \mathbf{S}_e\left(\mathbf{x}_e\right) + \frac{\partial S_{11}}{\partial E_{11}}\frac{\bar{A}_e}{\bar{L}_e^3}\mathbf{\Delta}\,\mathbf{x}_e\,\mathbf{x}_e^\intercal\,\mathbf{\Delta}, \tag{5}$$

where $^\intercal$ denotes the transpose operation and

$$E_{11} = \frac{1}{2}\frac{L_e^2 - \bar{L}_e^2}{\bar{L}_e^2} \tag{6}$$

is the component of the Green-Lagrange strain tensor in the element axial direction. The element length is defined as the distance between the nodes and can be calculated from the following formula:

$$L_e^2 = \mathbf{x}_e^\intercal\,\mathbf{\Delta}\,\mathbf{x}_e. \tag{7}$$

The constitutive law for the cable element is defined in order to conventionally take into account the inability of the cables to sustain relevant compressive stresses. To this aim, the

element is considered slack when the distance between its nodes is less than the element reference length. In such a case, the axial stress is assumed null. Otherwise, we assume a linearly elastic relationship between the Green-Lagrange strain and second Piola-Kirchhoff stress:

$$S_{11} = \begin{cases} EE_{11}, & \text{if } E_{11} \geq 0; \\ 0, & \text{otherwise;} \end{cases} \tag{8}$$

where E is the Young's modulus of the material.

A simple lumped mass matrix is considered for each element [22]:

$$\mathbf{M}_e = \frac{1}{2}\bar{\rho}_e \bar{A}_e \bar{L}_e \begin{bmatrix} \mathbf{I} & \mathbf{0} \\ \mathbf{0} & \mathbf{I} \end{bmatrix}, \tag{9}$$

where $\bar{\rho}_e$ is the (uniform) mass density in the reference configuration.

2.3. Governing equations

The nonlinear dynamic problem for the deployable cable net is governed by the following differential equation set:

$$\mathbf{M}\ddot{\mathbf{x}} + \mathbf{D}\dot{\mathbf{x}} + \mathbf{S}(\mathbf{x})\,\mathbf{x} = \mathbf{p}(t), \tag{10}$$

where $\mathbf{M}$, $\mathbf{D}$, and $\mathbf{S} \in \mathbb{R}^{3n\times 3n}$ respectively are the mass, damping, and secant stiffness matrices of the system, $\mathbf{x} = \mathbf{x}(t)$ is the nodal position vector in the current configuration at time t, and $\mathbf{p}(t)$ is the nodal load vector at time t. Here and in the following, the upper dot denotes differentiation with respect to time.

The mass and stiffness matrices of the system are obtained by assembling the corresponding matrices of the elements:

$$\mathbf{M} = \sum_{e=1}^{m} \mathbf{A}_e^{\intercal}\, \mathbf{M}_e\, \mathbf{A}_e \tag{11}$$

and

$$\mathbf{S}(\mathbf{x}) = \sum_{e=1}^{m} \mathbf{A}_e^{\intercal}\, \mathbf{S}_e(\mathbf{x}_e)\; \mathbf{A}_e. \tag{12}$$

The damping matrix is calculated according to Rayleigh's hypothesis [22]:

$$\mathbf{D} = \alpha\, \mathbf{M} + \beta\, \mathbf{T}(\bar{\mathbf{x}}), \tag{13}$$

where α and β are suitable combination coefficients and

$$\mathbf{T}(\bar{\mathbf{x}}) = \sum_{e=1}^{m} \mathbf{A}_e^{\intercal}\, \mathbf{T}_e(\bar{\mathbf{x}}_e)\; \mathbf{A}_e \tag{14}$$

is the tangent stiffness matrix of the system evaluated in the reference configuration.

3. Numerical example

3.1. Numerical solution method

The governing equations are integrated numerically by using the Runge-Kutta method with a variable time step, as implemented in the *ode45* solver available in MATLAB [23]. To this aim, the second-order equation set (10) is transformed into the following first-order equation set:

$$\dot{\mathbf{x}}(t) = \mathbf{v}(t) \tag{15}$$

$$\dot{\mathbf{v}}(t) = \mathbf{M}^{-1}\{\mathbf{p}(t) - \mathbf{S}[\mathbf{x}(t)]\; \mathbf{x}(t) - \mathbf{D}\,\mathbf{v}(t)\} \tag{16}$$

with the initial conditions at $t = 0$:

$$\mathbf{x}\,(0) = \mathbf{x}_0 \text{ and } \mathbf{v}\,(0) = \mathbf{v}_0. \tag{17}$$

The numerical example intentionally disregards some issues – such as gravitational and centrifugal forces – which will be included in future simulations. Thus, $\mathbf{p}\,(t) = 0$.

3.2. Energy balance

For the simplified problem considered, the total mechanical energy of the system, E_T, is the sum of two contributions: the kinetic energy,

$$K = \frac{1}{2}\mathbf{v}^{\intercal}\,\mathbf{M}\,\mathbf{v}, \tag{18}$$

and the elastic potential energy [20],

$$U_{el} = \frac{1}{2}\sum_{e=1}^{m} S_{11}E_{11}\;\bar{A}_e\bar{L}_e. \tag{19}$$

In the absence of damping, the total energy is expected to be constant over time. Otherwise, it will be a monotonically decreasing function of time. Checking the occurrence of these conditions can be exploited to test the accuracy of the obtained numerical solution.

3.3. Deployment of a planar cable net

As a very first illustrative example, we present the simulation of the in-plane deployment of a planar, square-mesh net whose reference configuration is depicted in Fig. 3. The geometry and material properties are taken from the study by Botta et al. [15] and resumed in Table 1. The net is formed by 5×5 square meshes of equal size. The cables have constant, circular cross sections. Four bullet masses are placed at nodes $1-4$ and are connected by strings to the corner nodes of the net. The model accounts for a total of 40 nodes and 64 elements.

As for the initial conditions, we consider a packed configuration of the net corresponding to 10% of the reference configuration: $\mathbf{x}_0 = 0.06\,\bar{\mathbf{x}}$. Initial velocities equal in magnitude to $v_b = 2.5$ m/s are given to the bullet masses in the radial directions. The Rayleigh damping coefficients are assumed as $\alpha = 10^{-3}$ s^{-1} and $\beta = 10^{-8}$ s.

Table 1. Geometry and material properties of the cable net.

Property	Symbol	Value	Unit
Net size	L	5	m
Mesh size	l	1	m
Corner string length	l_s	$\sqrt{2}$	m
Net cable diameter	d	0.002	m
Corner string diameter	d_s	0.004	m
Bullet mass	m_b	0.5	kg
Cable density	ρ	1390	kg/m^3
Young's modulus	E	70	GPa

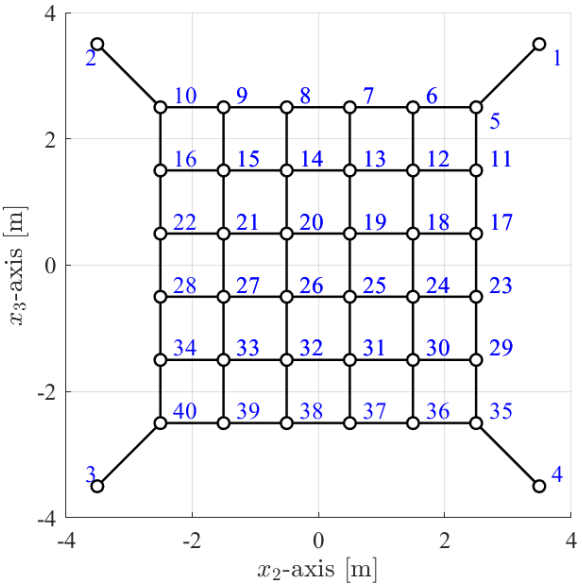

Figure 3. Planar cable net in the reference configuration.

3.4. Results

Figure 4 illustrates the simulated in-plane deployment of the cable net by showing its current configurations at six increasing instants of time: from the initial, packed configuration (at $t = 0$ s) to the quite fully deployed configuration (at $t = 2$ s). The deployment is achieved by ejecting the four bullet masses, linked to the corners of the net. When the strings connected to the bullets start tensioning, they pull along the neighbouring portions of the net.

Figure 5 shows the magnitudes of the four bullet velocities as functions of time. The overall decreasing trends testify the progressive transfer of energy from the bullets to the net. In particular, the sudden drops correspond to the conversion of the kinetic energy of the bullets into the elastic potential energy of the strings. We observe that for $t > 1.75$ s, the four curves start separating from each other. This result is not expected from the theoretical mechanical model and can be ascribed to a loss of accuracy of the numerical solution. Looking back at Fig. 4, we may correspondingly notice a loss of symmetry in the configurations reached by the cable net at about two thirds of its reference area.

Figure 6 presents the trends in time of the kinetic and elastic potential energies normalised with respect to the total mechanical energy, E_{T0}, evaluated at $t = 0$. A large number of narrow peaks are visible in the curve of the elastic potential energy. Correspondingly, narrow valleys are present in the curve of the kinetic energy. This correspondence testifies the conversion of the mechanical energy occurring during the net deployment. Besides, the decreasing trend of the superior envelope curve highlights the energy dissipation due to structural damping.

4. Conclusions

The development of accurate and effective simulation tools is crucial for the design of deployable cable nets for ADR missions.

We have proposed a FE model of a cable net with lumped nodal masses and first-order cable elements. In line with the ANCF, nodal positions have been adopted as the main unknowns of the problem. As a result, the elastic secant stiffness matrix of the system has turned out to be symmetric. The large displacements and finite deformations have been considered through the Green-Lagrange strain tensor. The cable elements have been assumed to react only in tension with a linear relationship between the axial strain and the corresponding component of the work-conjugate second Piola-Kirchhoff stress tensor. Global damping has been introduced

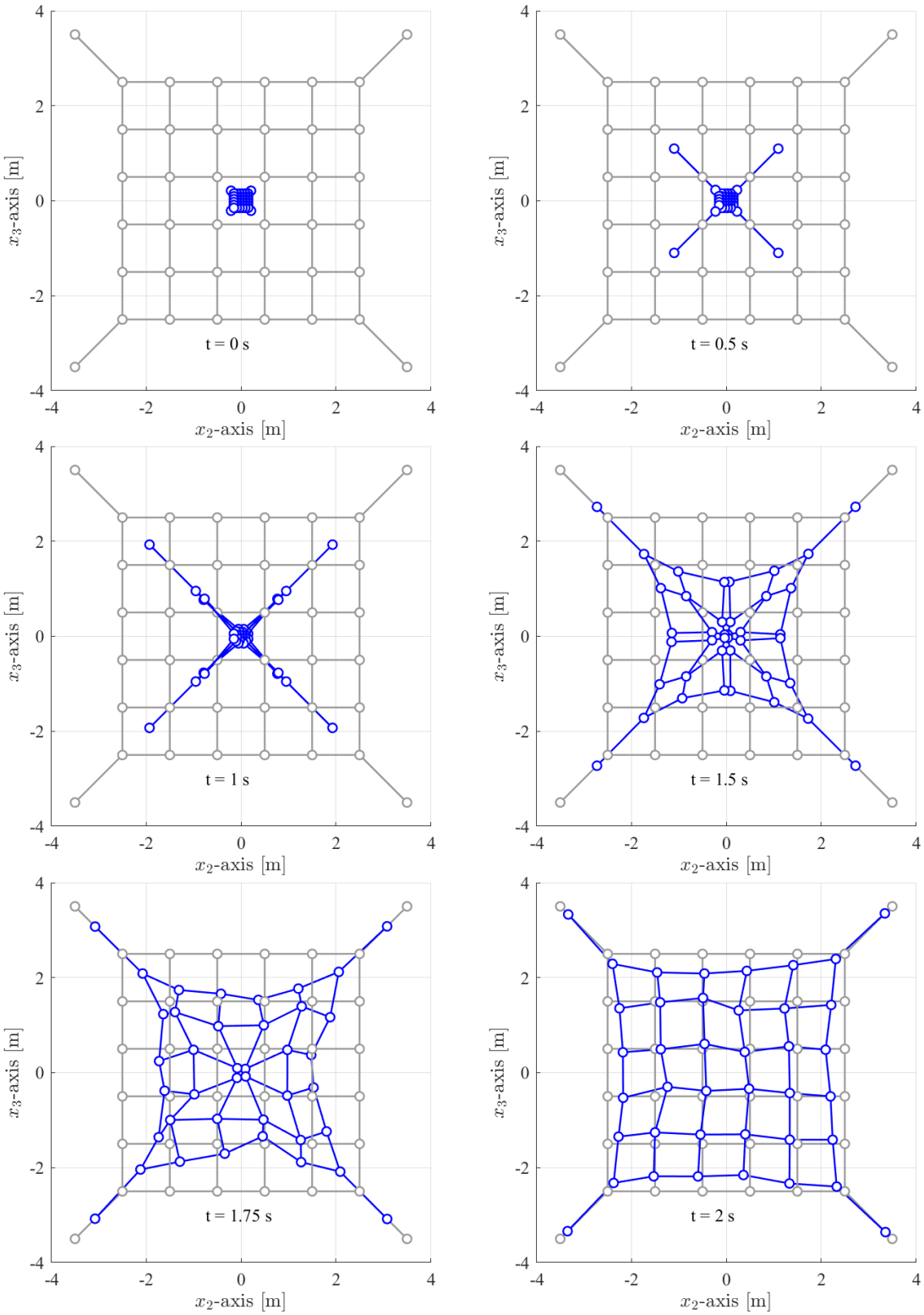

Figure 4. In-plane deployment of the cable net. Grey and blue lines represent the reference and current configurations, respectively.

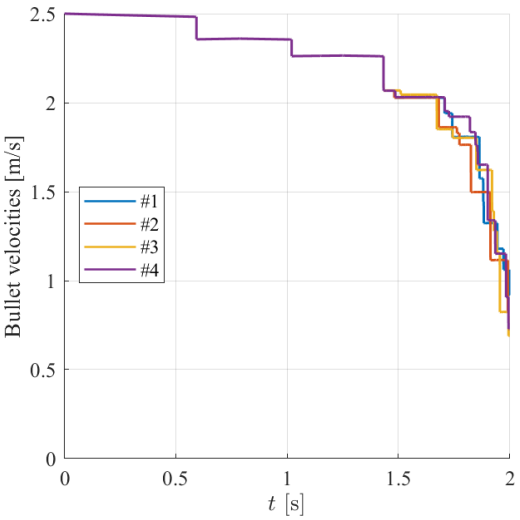

Figure 5. Velocities of the four bullet masses vs. time.

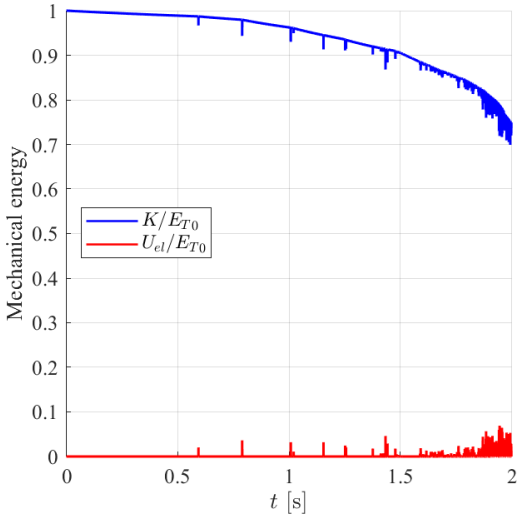

Figure 6. Kinetic and elastic potential energies vs. time.

into the model according to Rayleigh's hypothesis. The governing equations have been solved numerically by means of the Runge-Kutta method with a variable time step.

As an example, we have simulated the in-plane deployment of a planar, square-mesh net. The obtained results are reasonable, and the proposed approach is computationally efficient. Nonetheless, the numeral integration shows a loss of accuracy when the net reaches a deployment of about two thirds of its reference area. From this point of view, we will consider the adoption of a more efficient time integration algorithm.

Even though the presented results concern an example of in-plane deployment only, our model can already be used to compare several net configurations. In the literature, four parameters have been identified to evaluate the performance of a cable net in the deployment phase [15, 16]. They are the largest area the net comes out to reach during deployment, the time necessary to obtain it, the distance travelled in this time by the centre of mass of the net, and the time interval during which the actual area of the net is over 80% of its maximum achievable value. For a given net, our model can be used to evaluate the performances due to several throwing conditions, and to establish accordingly design factors for ADR missions.

To improve the plausibility of the simulation, we shall evaluate the order of magnitude of the main external forces and include the most significant ones into the theoretical model. Also, any centrifugal and Coriolis forces arising from the adoption of a non-inertial reference frame should be taken into account. Anyway, since the complete deployment of the net is attained in few seconds, the simulations from the simplified models may also be both efficient and reasonable computationally.

Lastly, the theoretical model shall be enriched to account for the relevant contact phenomena arising after the impact of the net with the target.

References

[1] National Research Council 1995 Hazards to space operations from debris *Orbital debris: A technical assessment* (Washington, DC: The National Academies Press)

[2] Kessler D J and Cour-Palais B G 1978 Collision frequency of artificial satellites: The creation of a debris belt *J Geophys Res* **83** 2637 – 46

[3] Kessler D J, Johnson N L, Liou J-C and Matney M 2010 The Kessler syndrome: Implications to future space operations *Proc. Conf. on Guidance and Control (Breckenridge, Colorado)* 47 – 62 (San Diego: American Astronautical Society)

[4] Inter-Agency Space Debris Coordination Committee 2021 *IADC space debris mitigation guidelines* IADC-02-01, Revision 3.
[5] Inter-Agency Space Debris Coordination Committee 2021 *Support to the IADC space debris mitigation guidelines* IADC-04-06, Revision 5.8.
[6] Pardini C and Anselmo L 2021 Evaluating the impact of space activities in low earth orbit *Acta Astronaut* **184** 11 – 22
[7] McKnight D S and Di Pentino F R 2013 New insights on the orbital debris collision hazard at GEO *Acta Astronaut* **85** 73 – 82
[8] Undseth M, Jolly C and Olivari M 2020 Space sustainability: The economics of space debris in perspective *OECD Science, Technology and Industry Policy Papers* **87** (Paris: OECD Publishing)
[9] Baranov A A, Grishko D A, Shcheglov G A, Sholmin A S, Stognii M V and Kamenev N D 2021 Feasibility analysis of LEO and GEO large space debris de/re-orbiting taking into account launch mass of spacecraft-collector and its configuration layout *Adv Space Res* **67** 371 – 83
[10] Liou J-C, Johnson N L and Hill N M 2010 Controlling the growth of future LEO debris populations with active debris removal *Acta Astronaut* **66** 648 – 53
[11] Shan M, Guo J and Gill E 2016 Review and comparison of active space debris capturing and removal methods *Prog Aerosp Sci* **80** 18 – 32
[12] Mark C P and Kamath S 2019 Review of active space debris removal methods *Space Policy* **47** 194 – 206
[13] Virgili-Llop J and Romano M 2019 Simultaneous capture and detumble of a resident space object by a free-flying spacecraft-manipulator system *Front Robot AI* **6** 1 – 14
[14] Benvenuto R, Salvi S and Lavagna M 2015 Dynamics analysis and GNC design of flexible systems for space debris active removal *Acta Astronaut* **110** 247 – 65
[15] Botta E M, Sharf I and Misra A K 2017 Energy and momentum analysis of the deployment dynamics of nets in space *Acta Astronaut* **140** 554 – 64
[16] Shan M, Guo J and Gill E 2017 Deployment dynamics of tethered-net for space debris removal *Acta Astronaut* **132** 293 – 302
[17] Shabana A A 1998 Computer Implementation of the Absolute Nodal Coordinate Formulation for Flexible Multibody Dynamics *Nonlin Dyn* **16** 293 – 306
[18] Gerstmayr J and Shabana A A 2006 Analysis of Thin Beams and Cables Using the Absolute Nodal Coordinate Formulation *Nonlin Dyn* **45** 109 – 30
[19] Wriggers P 2008 *Nonlinear Finite Element Methods* (Berlin: Springer)
[20] Valvo P S 2022 Derivation of symmetric secant stiffness matrices for nonlinear finite element analysis *Adv Sci Technol Res J* **22**
[21] Ogden R W 1984 *Non-linear Elastic Deformations* (Chichester: Ellis Horwood)
[22] Clough R W, Penzien J 2003 *Dynamics of Structures, 3rd ed.* (Berkeley: Computers & Structures)
[23] The MathWorks, Inc. 2021 *User's Guide* (r2021b)